Trapped Dust in HERA and Prospects for PEP-II *

Frank Zimmermann

Stanford Linear Accelerator Center,
Stanford University, Stanford, CA 94309

April 12, 1994

Abstract

A sudden reduction of the electron beam lifetime frequently observed in the HERA electron ring at DESY is attributed to the capture of charged macroparticles ('dust'). The effect may have implications for the design and assembly of the PEP-II High Energy Ring. In this report it is shown that the typical diameter of a trapped dust particle in HERA is about one micron and that it is most likely made from silicon dioxide. Mass, equilibrium charge and evaporation rate of such macroparticles are calculated, and two possible sources of dust, namely the distributed ion pumps and collection from the bottom of the beam pipe, are discussed. The potential for capturing dust by the beam and the evaporation rate of trapped particles are subsequently estimated for PEP-II. A simulation study confirms that trapped particles in HERA and PEP-II are dynamically stable for sufficiently large mass-to-charge ratio. However, thanks to the much higher beam current, they will be thermally unstable and evaporate rapidly in PEP-II. Furthermore, it is demonstrated that copper sputtering on the vacuum chamber wall cannot lead to an avalanche-like generation of copper ions in PEP-II.

1 Introduction

In 1992 and 1993, the HERA electron ring at DESY has suffered from regular sudden drops of the beam lifetime, which have limited the beam current for luminosity runs to values below 20 mA. In an earlier report [1] all observations at HERA could be explained by the capture of charged macroparticles of typically micron size. Since then, new machine experiments have been performed, which have proven, in particular, that the lifetime problem is related to the distributed ion pumps.

The successful operation of PEP-II requires currents of 1 A or above, a factor 50 higher than what has presently been achieved in HERA. The vacuum chamber design and the (original) pump design of PEP-II are almost identical to chamber and pumps at HERA. Therefore, a full understanding of the HERA problem appears essential in order to extrapolate to PEP-II conditions, to take precautions and to change the design of certain components, if necessary.

*Work supported by the Department of Energy, contract DE-AC03-76SF00515

This report aims to present a comprehensive and consistent theory of the most important aspects of dust trapping. Several topics, such as thermal properties of trapped particles, discharging processes and beam lifetime due to trapped dust, are compeletely revised and earlier assumptions had to be abandoned. More precisely, it will be shown that all particles with radius smaller than about one micron acquire the same temperature when trapped in the beam. As a consequence of the increased temperature of these particles (compared with Ref. [1]), field evaporation becomes the most important discharging process. It is interesting that a single trapped macroparticle which causes a beam lifetime of 30 minutes may be hundred times smaller than estimated previously. Most beam electrons are then lost due to 'duststrahlung', which is bremsstrahlung in the external field of the charged particle. Also silicon dioxide is now included in the list of possible constituents of a macroparticle. These modifications will lead to the conclusion that a single dust particle gives rise to the bad lifetime in HERA rather than a few hundred, which is a notable difference to Ref. [1] and is supported by the observations of 1993.

2 Lifetime Limitation at HERA

In 1992, a sudden reduction of the electron beam lifetime in HERA to less than 30 minutes was observed whenever the beam current exceeded a 'threshold' current of about 10 mA and 3 mA at an energy of 12 GeV and 26.5 GeV, respectively. The lifetime approached a constant value of less than 30 minutes and did not decrease further during continued injection. It showed a remarkable hysteresis-like behavior and stayed bad for currents much smaller than the 'threshold'. Only at very small currents, below 1 mA, there was evidence for a slight recovery. If a beam with a short lifetime at low current was dumped and immediately afterwards an electron beam of comparable current was re-injected, the lifetime of the latter was satisfactory (see Fig. 1).

With the help of loss monitors [2, 3], the beam loss, due to bremsstrahlung, was localized in a 20 m long section. After the exchange of this part of the beam pipe it was possible to store electron currents up to 29 mA at 12 GeV towards the end of 92.

However, in 1993 a similar drop of beam lifetime occurred frequently for currents larger than 20 mA. The loss rates were always localized in short sections of the ring. Often the loss rates were observed to travel in the direction of the beam (at velocities of about 100–1000 m/s) and to disappear after typically 10 s, while the irreversible lifetime reductions corresponded to stationary losses. Observations of 1993 indicate that there is no clearly defined threshold of energy and/or current, but that instead the probability of the effect strongly depends on these two parameters. Important progress has been made at the end of 93, when it was shown that switching off or reducing the voltage of the distributed ion pumps in the dipole magnets leads to a disappearance of the irreversible breakdowns of lifetime, at least for currents up to 29 mA. Early in 1994, a lot of small craters were found on the anode plates of the distributed ion pumps, and in some of them macroparticles consisting of silicon dioxide. The origin of the silicon dioxide is unclear. It is either a relic from special cleaning procedures (for instance sandblasting) or debris from the tunnel walls (e. g. concrete) [4].

The observations indicate that ionized particles are trapped by the beam. Since neither a coherent nor an incoherent tune shift is measured, their mass-to-charge ratio must be much larger than that of single-atomic ions. It is, furthermore, interesting that coherent transverse oscillations (induced by switching off the multi-bunch feedback system) lead to a significant

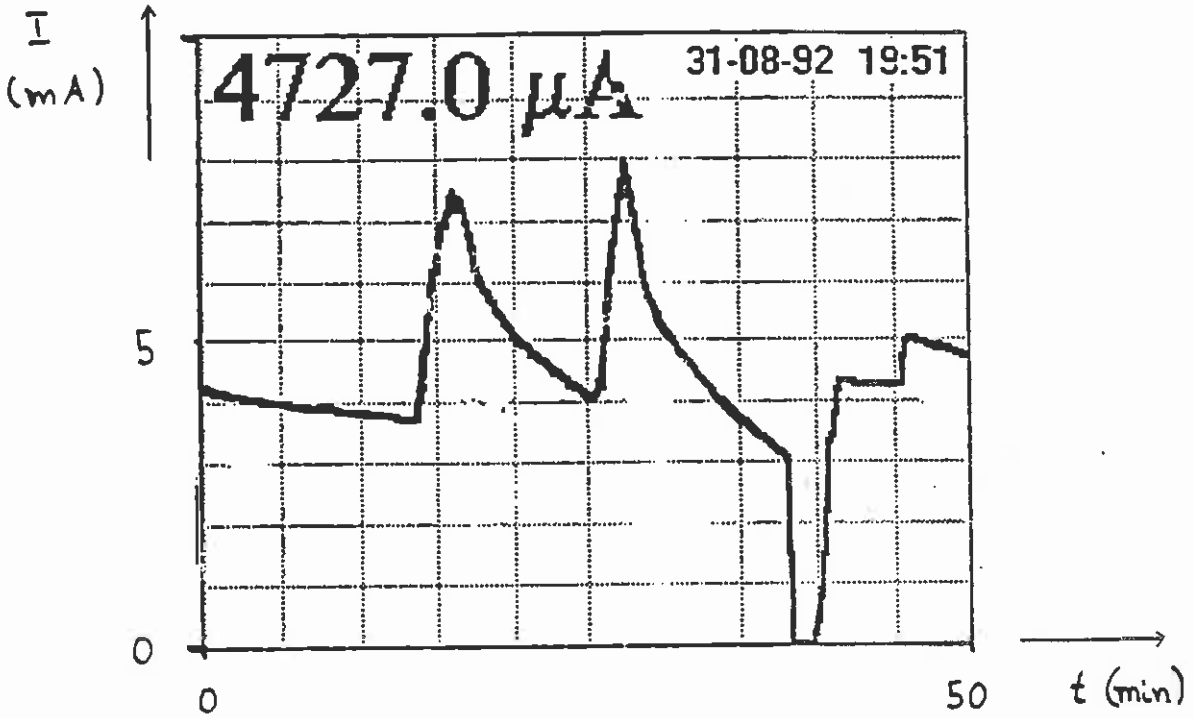

Figure 1: Decrease of the beam lifetime in the HERA electron ring if a certain threshold current has been exceeded and recovery of the lifetime after beam dump and new injection.

increase in beam lifetime, while re-activating the feedback causes the lifetime to drop to its original small value [4]. A current limitation, very similar to HERA, is also being observed in DORIS, which offers the additional possibility to compare the lifetime of an electron beam with that of a positron beam circulating in the opposite direction. Positrons do not show the sudden decrease in lifetime, which supports the hypothesis that positively charged particles are trapped by the electron beam.

Both HERA and DORIS are equipped with a copper vacuum chamber and with the same type of distributed ion pumps (plate design, anodes at high voltage). In PETRA, where sudden reductions of the electron beam lifetime have not been seen, pumps and vacuum chamber are different. It is worthwhile to note that beam loss phenomena ascribed to dust trapping have also been observed in the TRISTAN accumulation ring [5, 6], in DCI and Super-ACO [7], in CESR [8] and in the CERN Antiproton Accumulator [9]. A 'dust problem' is even reported from AdA, the first electron-positron collider in operation, as early as 1961 [10].

3 Parameters of Storage Rings and Substances

Table 1 compares various machine parameters of HERA and DORIS, at which a drop of beam lifetime is typically observed, with those envisioned for PEP-II. The most important difference of PEP-II is the, by a factor 10–50 larger, beam current, which will lead to significant consequences in the following analysis.

Among other quantities, electric fields and the beam potential are listed. They have been calculated as follows. The electric field at one sigma is given by

$$E_{x,y}(\sigma_{x,y}) \approx \frac{N_{el}^{tot} e}{2\pi\epsilon_0(\sigma_x + \sigma_y)C}, \tag{1}$$

while at the chamber wall it is

$$E(d) \approx \frac{N_{el}^{tot} e}{2\pi\epsilon_0 dC} \tag{2}$$

where $d \equiv \sqrt{d_x d_y}$. The potential at the center of the beam reads

$$U(0) \approx \frac{I}{4\pi\epsilon_0 C}\left(1 + 2\ln\frac{d}{a}\right), \tag{3}$$

strictly valid for a beam of uniform density and radius a. In the case of a flat Gaussian beam, we use equation (3) with $a \approx \sqrt{2\sigma_x\sigma_y}$.

Some properties of relevant materials are compiled in Table 2, for future reference. The HERA vacuum chamber is made from copper, while the PETRA chamber is manufactured from aluminum. These two materials have very similar properties. The distributed ion pumps contain titanium as getter material, which has a considerably larger thermal stability (lower vapor pressure) than copper or aluminum. The most stable material is silica, which was found on the pump electrodes in HERA. Moreover, silica is also the least dense of the materials considered and has the largest heat capacity.

A further interesting property of silica is that it undergoes various phase transitions when heated. So α-Quartz changes into β-Quartz at 848 K, into β_2-Tridymite at 1143 K, and at 1743 K into β-Cristobalite. These phase transitions are accompanied by a decrease in density from 2.65 g/cm^3 for α-Quartz to 2.21 g/cm^3 for β-Cristobalite [37]. The reduction of density has a stabilizing effect on a macroparticle trapped in the beam, since it increases the surface area and thus the ability for heat radiation, while the deposited ionization energy depends only on the total mass.

The temperature-dependence of the vapor pressure is customarily parametrized in the form

$$\log\frac{p}{\text{torr}} = -\frac{A}{T} + B + C\log T + DT. \tag{4}$$

The coefficients A–D depend on the units chosen. For the values in Table 2, the temperature is measured in K and the pressure in torr (1 torr $\approx$ 133 Pa). The coefficients for aluminum, copper and titanium are from Ref. [15], those for silica were obtained by a fit to data from Ref. [16] (dots).

The photon attenuation coefficients μ are taken from [12]. They describe the reduction of intensity of X-rays after a distance x in the medium,

$$\frac{I(x)}{I_0} = e^{-\mu\rho x} \tag{5}$$

Parameter	HERA	DORIS	PEP-II HER
beam energy and size			
electron energy E_e [GeV]	26.5	4.5	9
beam current I [mA]	20	100	1000
total number of electrons N_{el}^{tot}	$2.6 \cdot 10^{12}$	$6 \cdot 10^{11}$	$5 \cdot 10^{13}$
revolution frequency f_{rev} [kHz]	50	1000	150
revolution period t_{rev} [μs]	20	1	7
relativistic gamma γ_e	53 000	9000	1800
number of populated bunches n_{bunch}	100	5	1658
number of empty bunches n_{gap}	120	0	88
bunch spacing Δt [ns]	96	193	4.2
circumference C [m]	~ 6000	~ 290	2200
average beta function β [m]	~ 27	~ 15	25 (hor.), 20 (vert.)
horizontal beam size σ_x [mm]	1.0	2.3	0.85
vertical beam size σ_y [mm]	0.23	0.6	0.169
synchrotron radiation			
bend radius ρ_{bend} [m]	600	~ 50	165
radiation power per meter [W/m]	150	240	3000
number of photons [$m^{-1}s^{-1}$]	$7 \cdot 10^{16}$	10^{18}	$7 \cdot 10^{18}$
critical energy E_{crit} [keV]	42	4	10
electric fields and beam potential			
hor. half aperture d_x [mm]	~ 40	~ 40	45
vert. half aperture d_y [mm]	~ 20	~ 20	25
$E(1\sigma)$ [V/m]	970	2050	64 000
$E(d)$ [V/m]	30	149	1450
$U(0)$ [V]	5	20	280

Table 1: Comparison of PEP-II HER parameters with those of HERA and DORIS.

Substance	Aluminum	Copper	Titanium	Silica
A_{atom}	27	64	48	60
Z_{atom}	13	29	22	30
density $[\frac{g}{cm^3}]$	2.70	8.96	4.54	2.2–2.64
m.p. [K]	933	1352	1941	1983
b.p. [K]	2673	2853	3533	2503
heat capacity C_p [J mol^{-1}K^{-1}] (at 1500 K)	29.3	35.6	33.7	72.47
surface tension [mN m^{-1}]	840 (at 973 K)	1150 (at 1352 K)	1427 (at 1941 K)	
work function Φ_- [eV]	4.28	4.65	4.17	
ionization energy U [eV]	5.99	7.73	6.83	
vaporization energy V [eV]	3.1	3.2	4.5–4.9	
$\frac{dE}{dx}\|_{min}$ $[\frac{MeV}{g/cm^3}]$	1.62	1.44	1.51	1.72
coefficients for vapor pressure equation				
A	16 450	17 456	24 275	27 071
B	12.36	9.8022	10.663	10.861
C	-1.023	0	0	0
D	0	$-1.659 \cdot 10^{-4}$	$-2.3 \cdot 10^{-4}$	$-4.4 \cdot 10^{-4}$
photon attenuation coefficients				
μ $[\frac{cm^2}{g}]$ (1 keV)	$1.19 \cdot 10^3$	$1.06 \cdot 10^4$	$5.87 \cdot 10^3$	
μ $[\frac{cm^2}{g}]$ (10 keV)	$2.62 \cdot 10^1$	$2.16 \cdot 10^2$	$1.11 \cdot 10^2$	
μ $[\frac{cm^2}{g}]$ (100 keV)	$1.2 \cdot 10^{-1}$	$4.58 \cdot 10^{-1}$	$2.72 \cdot 10^{-1}$	

Table 2: Some properties of copper, carbon, titanium and silica [11, 12, 13, 14].

where I_0 is the initial intensity and ρ the mass density.

In the remainder of this report, the symbol

r_p	denotes the classical proton radius ($r_p \approx 1.5 \cdot 10^{-18}$ m),
r_e	the classical electron radius ($r_e \approx 2.8 \cdot 10^{-15}$ m),
c	the velocity of light,
Q	the charge of the particle in units of e,
A	the mass of the particle in units of the proton mass m_p , and
R	the radius of the particle.

4 Beam Lifetime Caused by a Trapped Macroparticle

If the beam loss is caused by bremsstrahlung in the field of the nuclei of the macroparticle, the beam lifetime τ_{beam} is written as [17]

$$\frac{1}{\tau_{beam}} \approx \left(\frac{16 r_{el}^2}{3 \cdot 137} \ln \frac{E_e}{\Delta E_e} \ln \frac{183}{(Z_{atom})^{\frac{1}{3}}} \right) \cdot c \cdot \frac{A (Z_{atom})^2}{A_{atom} 2\pi \sigma_x \sigma_y C} \tag{6}$$

where

r_e	is the classical electron radius ($r_e \approx 3 \cdot 10^{-15}$ m),
$\Delta E_e / E_e$	the energy acceptance ($\Delta E_e / E_e \sim 1/100$).
A_{atom}	the atomic mass, and
Z_{atom}	the atomic number of the constituents

In this case the beam lifetime is inversely proportional to the total mass trapped by the beam. To give rise to a beam lifetime of 30 minutes in HERA and the PEP-II HER and considering quartz as material, the required mass is

$$A \approx 4 \cdot 10^{14} \tag{7}$$

$$A \approx 1 \cdot 10^{14} \tag{8}$$

Bremsstrahlung can, however, also take place in the electric field of the charged dust particle as a whole. This process is similar to the beamstrahlung, familiar from linear colliders, and may be called 'duststrahlung' [18]. To estimate the order of magnitude of this effect, we calculate a dimensionless parameter $\Upsilon(b)$ known from the treatment of beamstrahlung [19, 20],

$$\Upsilon(b) \equiv \frac{\hbar c \gamma^3}{\rho E_e} \approx \frac{\hbar c^2 \gamma^3}{b E_e} \frac{\Delta p_{trans}}{E_e} \approx 1.1 \cdot 10^{-22} \cdot \frac{Q}{b^2} \text{ m}^2 \tag{9}$$

Here, $\rho \approx (E_e b)/(c\ \Delta p_{trans})$ is the local bending radius and $\Delta p_{trans} \approx (2Qe^2)/(4\pi\epsilon_0 c b)$ the transverse momentum transfer for impact parameter b. The numerical value applies to HERA. Assuming, for instance, a charge $Q = 10^9$ and impact parameter $b = 1$ μm, we find $\Upsilon \approx 0.11$. The average number $N_\gamma(b)$ of emitted photons per electron and per revolution time is [20]

$$N_\gamma(b) \approx \frac{5}{2\sqrt{3}} \frac{c\alpha \Upsilon(b)}{\lambda_e \gamma} \frac{1}{(1 + \Upsilon(b)^{\frac{2}{3}})^{\frac{1}{2}}} \cdot \frac{b}{c} \approx 9 \cdot 10^{-4} \tag{10}$$

where we have multiplied the rate of photons per unit time from Ref. [20] by the interaction time $\Delta t \approx \frac{b}{c}$. The number on the far right-hand side is obtained for $b = 1$ μm and $Q = 10^9$. The average photon energy is larger than $E/100$ (which is the energy acceptance of HERA) if $\Upsilon \geq 0.02$, corresponding to

$$b_{max} \approx 2.4 \ \mu\text{m} \quad (\text{for } Q = 10^9) \tag{11}$$

For $b < b_{max}$, the typical photon energy is so high that an electron is lost when it emits a photon. An effective cross section can then be introduced as

$$\sigma_{eff} \equiv \pi \int_{b_{min}}^{b_{max}} N_\gamma(b)\ b\ db \tag{12}$$

with $b_{min} \approx R$. The beam lifetime τ_{beam} is related to this effective cross section via

$$\sigma_{eff} \cdot \frac{c}{2\pi\sigma_x\sigma_y C} = \frac{1}{\tau_{beam}}. \tag{13}$$

To cause a beam lifetime of 30 minutes the required charge of a macroparticle ($R \approx 1$ μm) is approximately

$$Q \approx 6 \cdot 10^8 \ \text{ for both HERA and the HER.} \tag{14}$$

If the beam lifetime is due to duststrahlung, it is roughly proportional to $Q^{\frac{3}{2}}$ and relatively independent of the particle mass A.

5 Dynamic Stability

Denoting the vertical position and velocity of a particle by y and $\dot{y}$, respectively, the motion of a charged particle in the beam pipe can be approximately described by a succession of drifts and nonlinear kicks from individual bunches [21]. A drift represents the time interval between two bunch passages and has the simple form

$$\begin{pmatrix} y \\ \dot{y} \end{pmatrix}_{final} = \begin{pmatrix} 1 & \Delta t \\ 0 & 1 \end{pmatrix} \begin{pmatrix} y \\ \dot{y} \end{pmatrix}_{initial}, \tag{15}$$

while the kick by a bunch for the special case of a round beam of rms-size σ_r reads

$$\Delta\dot{y} = -\frac{N_{el}^{tot} 2 c r_p}{n_{bunch}} \frac{y}{r^2} \left(1 - \exp\left(-\frac{r^2}{2\sigma_r}\right)\right) \cdot \frac{Q}{A}. \tag{16}$$

where $r \equiv \sqrt{x^2 + y^2}$. The kick from a flat Gaussian beam is given by the Bassetti-Erskine formula [22]. In what follows we will only use the simpler round beam kick, whose evaluation is considerably faster and avoids numerical problems at very large amplitudes. As value for σ_r in the round beam kick we choose the vertical beam size σ_y for the stability studies presented here, and either the horizontal or the vertical beam size to study the kinetic energy of particles hitting the vacuum chamber wall in a section 10.

In order to determine the dynamic stability of trapped ionized particles, computer simulations have been performed, using (15) and (16). To give an example of the simulation results, Figures 2 and 3 show the vertical position as a function of time for an unstable and a stable

particle in the PEP-II HER, corresponding to two different mass-to-charge ratios. Due to the gap of 88 empty bunches, single atomic ions are dynamically unstable and are lost in less than five revolution periods.

Fig. 4 summarizes the results obtained for the PEP-II HER. Depicted is the minimum stable mass-to-charge ratio as a function of the vertical starting amplitude $y_{initial}$. The starting horizontal amplitude is chosen as zero ($x_{initial} = 0.0$). The capture of particles is determined by the value at large starting amplitudes ($y_{initial} \geq 2\sigma_y \approx 0.34$ mm). From the figure, the mass-to-charge-ratio of trapped particles in the PEP-II HER has to fulfill the condition

$$\frac{A}{Q} \geq 5 \cdot 10^4. \tag{17}$$

This is about the same border of stability as previously found for HERA [1].

The oscillation frequency in the linear region of the beam force (i.e. for oscillation amplitudes smaller than one sigma) is

$$f_{x,y} = \frac{1}{2\pi}\left(\frac{2c^2 r_p N_{el}^{tot} Q}{C\sigma_{x,y}(\sigma_x + \sigma_y)A}\right)^{\frac{1}{2}} \tag{18}$$

which for HERA gives

$$f_x = 1.5 \cdot 10^6 \sqrt{\frac{Q}{A}}\ \text{Hz} \quad , \quad f_y = 3.1 \cdot 10^6 \sqrt{\frac{Q}{A}}\ \text{Hz} \tag{19}$$

and for the PEP-II HER

$$f_x = 1.3 \cdot 10^7 \sqrt{\frac{Q}{A}}\ \text{Hz} \quad , \quad f_y = 2.9 \cdot 10^7 \sqrt{\frac{Q}{A}}\ \text{Hz} \tag{20}$$

Since A/Q for trapped macroparticles is of the order of 10^5, as shown later, their oscillation frequencies lie in the range between 1 and 100 kHz. Single-atomic ions, if stable, would oscillate at frequencies as high as $10^6 - 10^7$ Hz.

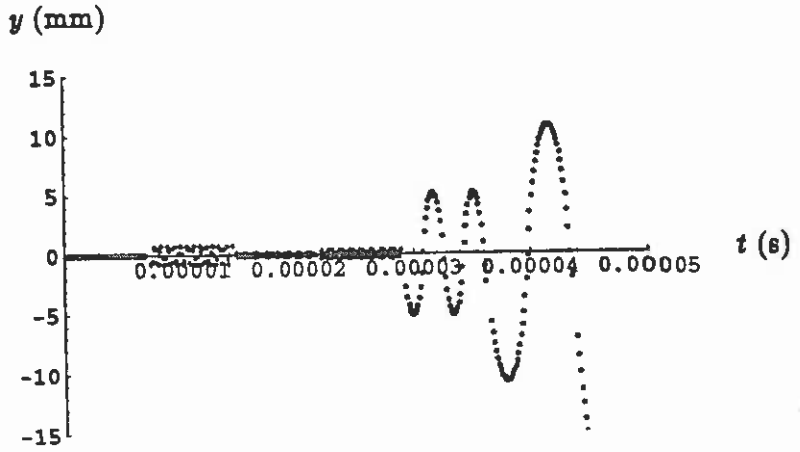

Figure 2: Vertical motion of unstable ion in the PEP-II HER for a mass-to-charge ratio A/Q = 100. The particle is launched at $y_{initial} = 0.1$ mm, $x_{initial} \approx 0$ ($\sigma_y = 0.169$ mm).

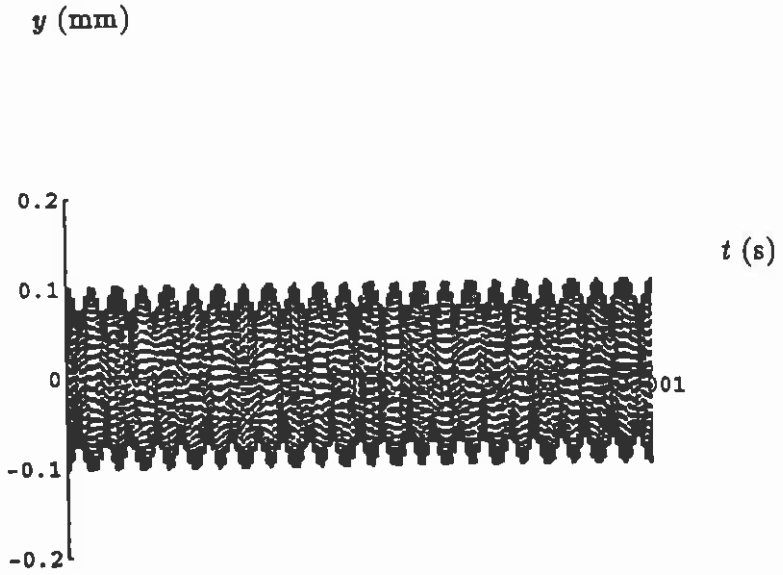

Figure 3: Vertical motion of a stable ion in the PEP-II HER for a mass-to-charge ratio A/Q = 10^5. The particle is launched at $y_{initial} = 0.1$ mm, $x_{initial} \approx 0$ ($\sigma_y = 0.169$ mm).

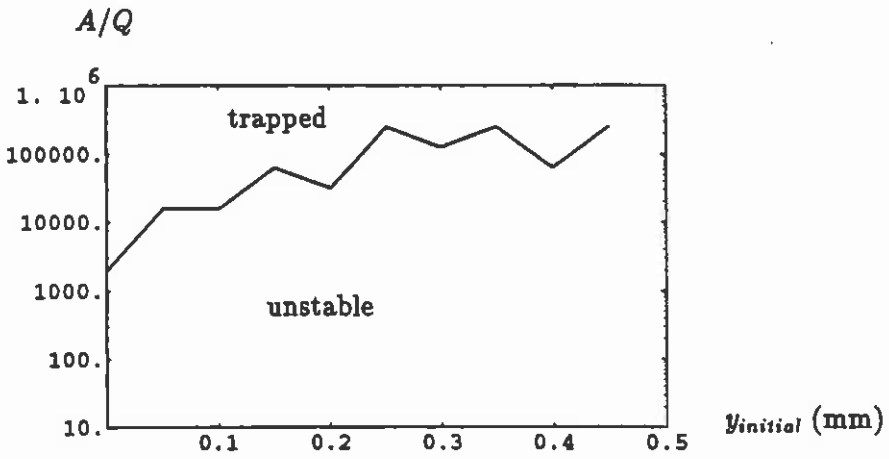

Figure 4: Minimum stable mass-to-charge ratio as a function of initial vertical amplitude, determined by a simulation study for the PEP-II HER.

6 Equilibrium Charge

A trapped macroparticle gets rapidly ionized by the beam, until discharging effects become equally strong so that some equilibrium is reached. One possibility to discharge is the capture of photoelectrons generated by the synchrotron radiation on the chamber wall. For high temperature and high charge another effect is considerably more important, namely the field evaporation of ions [23, 24, 8]. In the following, explicit expressions for these three rates are derived.

The distribution of secondary electrons with energy T large compared to the atomic ionization energy is given by [11]

$$\frac{d^2N}{dTdx} = 2\pi N_A r_e^2 m_e c^2 \frac{Z_{atom}}{A_{atom}} \frac{1}{T^2} \tag{21}$$

Here,

r_e	is the classical electron radius ($r_e \approx 3 \cdot 10^{-15}$ m),
m_e	the electron mass,
N_A	Avogadro's number,
A_{atom}	the atomic mass of the material, and
Z_{atom}	its atomic number.

The number of electrons which escape from the charged particle is proportional to $\int_{T_{min}}^{T_{max}} d^2N/(dTdx)$ where the lower limit of integration T_{min} is

$$T_{min} = \frac{Qe^2}{4\pi\epsilon_0 R}. \tag{22}$$

Then, for large values of Q the rate of ionization is approximately

$$\dot{Q}_{ioniz} \approx \frac{16\pi^2}{3} f_{rev} \cdot N_{el}^{tot} N_A r_e^2 m_e c^2 \frac{Z_{atom}}{A_{atom}} \frac{\epsilon_0}{e^2} \rho \frac{1}{\sigma_x \sigma_y} \frac{R^4}{Q}. \tag{23}$$

where ρ denotes the mass density of the material considered. The ionization rate (23) is proportional to the fourth power of the radius R and inversely proportional to the charge Q. In the case of silica we find

$$\dot{Q}_{ioniz} \approx 5 \cdot 10^{39} \left(\frac{R}{\mathrm{m}}\right)^4 \frac{1}{Q} \frac{1}{\mathrm{s}} \text{ for HERA} \tag{24}$$

$$\dot{Q}_{ioniz} \approx 3 \cdot 10^{41} \left(\frac{R}{\mathrm{m}}\right)^4 \frac{1}{Q} \frac{1}{\mathrm{s}} \text{ for the HER.} \tag{25}$$

Integration yields

$$Q \approx \sqrt{1 \cdot 10^{16} \frac{t}{\mathrm{s}} + Q_0^2} \quad \text{for HERA,} \tag{26}$$

$$Q \approx \sqrt{6 \cdot 10^{17} \frac{t}{\mathrm{s}} + Q_0^2} \quad \text{for the HER,} \tag{27}$$

assuming a radius $R = 1\mu$m; Q_0 is the charge at time $t = 0$.

The ionization (23) is balanced by discharging processes, and the charge Q approaches an equilibrium value. One discharging effect is the capture of photoelectrons which are created by

synchrotron radiation-induced photoemission from the vacuum chamber. To estimate its order of magnitude we will roughly follow reference [8]. The discharging rate is approximately given by

$$\dot{Q}_{disc} \approx -\frac{1}{\tau_{pe}} \frac{\bar{\sigma}_{pe}}{\pi d C}. \tag{28}$$

Here,

$1/\tau_{pe}$	is the photoelectron creation rate,
$\bar{\sigma}_{pe}$	the mean capture cross section, and
d	the radius of the vacuum chamber.

The photoelectron creation rate is expressed as [8]

$$\frac{1}{\tau_{pe}} \approx 10^{-2} \frac{\bar{\mu} \gamma c N_{el}^{tot}}{\rho_{bend}}, \tag{29}$$

where $\bar{\mu}$ is the mean electron yield per photon averaged over the photon spectrum. The value of $\bar{\mu}$ is known only, say, within an order of magnitude and depends sensitively on the properties of the vacuum chamber surface. The mean capture cross section which is enhanced by the electric charge of the dust particle is roughly [8]

$$\bar{\sigma}_{pe} \approx \pi R^2 \frac{T_{min}}{E_{pe,max}} \ln\left(\frac{E_{pe,max}}{E_{pe,min}}\right) \tag{30}$$

Following [8], the maximum and minimum photoelectron energies $E_{pe,max}$, $E_{pe,min}$ are chosen as 100 eV and 0.1 eV, respectively. Then, for a vacuum chamber radius $d \approx 3$ cm and assuming $\bar{\mu} = 0.05$, the discharging rate for HERA at 26 GeV is

$$\dot{Q}_{disc} \approx -1.7 \cdot 10^7 \, Q \left(\frac{R}{\mathrm{m}}\right) \frac{1}{\mathrm{s}}. \tag{31}$$

The second discharging process, which will be the dominant one for high charge and high temperature, is the field evaporation of ions. It is described by an equation similar to the Richardson-Dushman equation for thermionic emission of electrons [13],

$$\begin{aligned} \dot{Q}_{ev} &= -\frac{A_{atom} m_p 8\pi^2 R^2 k_B^2}{h^3} T^2 \cdot \\ &\quad \cdot \exp\left(-\frac{U+V-\Phi_-}{k_B T} + \frac{e^2\sqrt{Q}}{4\pi\epsilon_0 R k_B T} - \frac{1}{k_B}\int_0^T \frac{dT'}{T'^2}\int_0^{T'} dT''\, C_p(T'')\right) \end{aligned} \tag{32}$$

where C_p is the heat capacity at constant pressure of an ion in the condensed state, U is the ionization energy, V the vaporization energy and Φ_- the work function of the material. The double integral over the heat capacity will be approximated as

$$\int_0^T \frac{dT'}{T'^2}\int_0^{T'} dT''\, C_p(T'') \approx \frac{C_p}{k_B} \ln\left(\frac{T}{T_0}\right) \tag{33}$$

where for titanium we have $T_0 \approx 1500$ K and $C_p \approx 33/N_A$ J/K [16].

As an illustration, Fig. 5 presents the absolute value of the charging rate (23) and the discharging rates (28) and (65) as a function of the charge Q, for a titanium particle of radius

$R \approx 1\mu$m at the temperature 1500 K. The equilibrium charge is determined by the intersection of the ionization rate and the steeply increasing (as a function of charge) field evaporation. The photoelectron capture is too small to be significant for this set of parameters. It may become important, however, for lower temperature or larger radius. Due to the large slope of $\dot{Q}_{ev}(Q)$ the charge of a trapped particle is almost independent of the beam current. Consequently, the beam lifetime, caused by duststrahlung, stays approximately constant for decreasing current, which is consistent with the observations. The equilibrium charge of $Q \approx 10^7$ is in remarkable agreement with the charge causing a beam lifetime of 30 minutes due to duststrahlung.

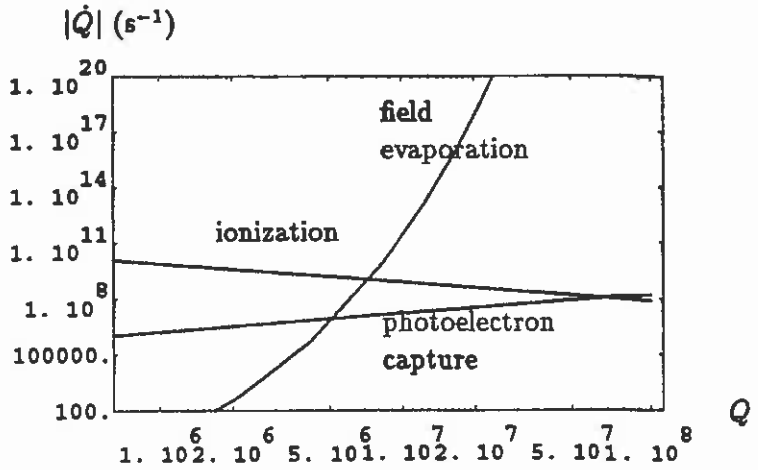

Figure 5: Charging and discharging rates for a titanium particle of radius $R \approx 1$ μm at temperature 1500 K in HERA. For the discharging rate by photo-electron capture a mean photoelectron yield of $\bar{\mu} = 0.05$ has been assumed.

Once its charge and radius are known, the value of the surface tension γ_{surf} determines if a molten particle is stable. More explicitly, the condition for stability is

$$4\pi R^2 \gamma_{surf} > \frac{Q^2 e^2}{4\pi\epsilon_0 R} \tag{34}$$

which translates into a condition for A/Q^2,

$$\frac{A}{Q^2} > \frac{e^2}{12\pi\epsilon_0 m_p} \frac{\rho}{\gamma_{surf}} \approx 145 \tag{35}$$

where the numerical value applies to aluminum and titanium. Hence, for typical equilibrium charges and masses ($A \approx 10^{12} - 10^{14}$, $Q \approx 10^7 - 10^8$) the particles will not be stable, but explode when they approach their equilibrium (typically in much less than a second). Only those particles are stable, whose equilibrium temperature is below their melting point [25]. We shall see later, that from all the materials considered, nothing but silicon dioxide fulfills this criterion.

7 Sources of Dust

7.1 Distributed Ion Pumps

It is well known [26, 27, 28, 29] that vacuum arcs are accompanied by the production of low-charged macroparticles of a typical size $0.1 - 1\mu$m, emitted from both cathodes and anodes. Vacuum arcs are occasionally observed in distributed ion pumps. Even in the absence of electric discharges, the ion pumps in a storage ring will contain a certain number of dust particles (e. g. debris). If macroparticles exist or are generated by a vacuum arc inside the distributed ion pumps, they may be charged either from the beginning or by synchrotron radiation, and accelerated in the direction of the pump slots by the applied voltage (about 5 kV in HERA). The pump slots are located at about the same height as the beam, separated from the latter by the horizontal half-aperture $d_x \sim 45$ mm. Dependent on their initial velocity (and hence on the pump voltage U_p and initial charge Q_0) and their mass, the macroparticles may either fall down, or cross the beam and hit the other side of the chamber, or be trapped by the beam. We want to derive some crude formulae to see when the particles are trapped. The initial velocity is given by

$$v_{x,0} = \left(\frac{2eQ_0U_p}{Am_p}\right)^{\frac{1}{2}} \tag{36}$$

One condition for capture is that the particle has not fallen by more than about 8 vertical σ_y at the time when it reaches the horizontal beam position. The factor 8 comes from a simulation study. This condition translates into

$$\frac{A}{Q_0} \leq 4 \cdot 10^4 \, \frac{U_p}{\mathrm{kV}} \tag{37}$$

The second condition stems from the requirement that the particle crossing the beam is ionized so much that it is trapped. The change of charge during the (first) beam crossing is roughly given by

$$\Delta Q = \dot{Q}_{ioniz} \frac{2\sigma_x}{v_{x,0}} \tag{38}$$

and the second condition then reads

$$(Q_0 + \Delta Q) \cdot U(0) \geq Q_0 U_p \tag{39}$$

where $\dot{Q}_{ioniz}$ was calculated in (23) and U_0 is the potential at the bunch center, given in Table 2. Evaluation yields

$$\frac{A^{\frac{11}{3}}}{Q_0^5} \geq 2.2 \cdot 10^{24} \left(\frac{U_p}{\mathrm{kV}}\right)^3 \text{ for HERA} \tag{40}$$

$$\frac{A^{\frac{11}{3}}}{Q_0^5} \geq 1.2 \cdot 10^{22} \left(\frac{U_p}{\mathrm{kV}}\right)^3 \text{ for the PEP-II HER} \tag{41}$$

The particle masses which are suited for capture are depicted in Fig. 6 as a function of initial charge Q_0 for a pump voltage of 5 kV. Note that we have assumed pump slots at the same height as the beam and horizontal direction of motion when the particles are emitted from the pump slots. Even for the unlikely emission angle of 45 degree or vertical separation of beam

and slots equal to the vertical half-aperture, the resulting mass values differ by not more than a factor of ten. Simulation studies indicate that our inequalities may be somewhat too loose, since, in particular for high initial charges, less particles are found to be trapped than expected from (37) and (39). As an illustration, a simulation result for a successful capture is shown in Fig. 7.

In order to avoid the emission of charged particles from the pumps in the HER it has been proposed [30] to change the design of the distributed ion pumps to a so-called 'reversed-ground' type. Here, the central anode plates are on the same (ground) potential as the vacuum chamber, while the cathodes are at negative high voltage. Acceleration of positive macroparticles through the pump slots then becomes impossible.

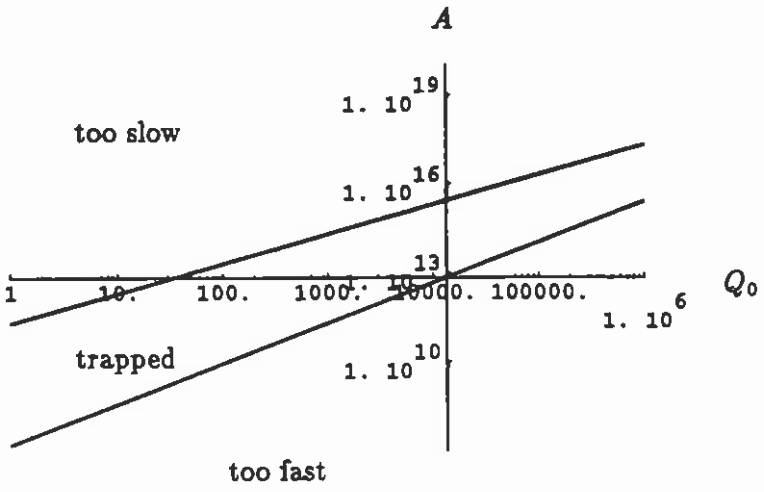

Figure 6: Mass A which can be trapped by the HERA electron beam, for macroparticles accelerated by an ion pump of voltage 5 kV, as a function of initial charge Q_0. The two lines represent inequalities (37) and (39). Particles between these lines can be captured.

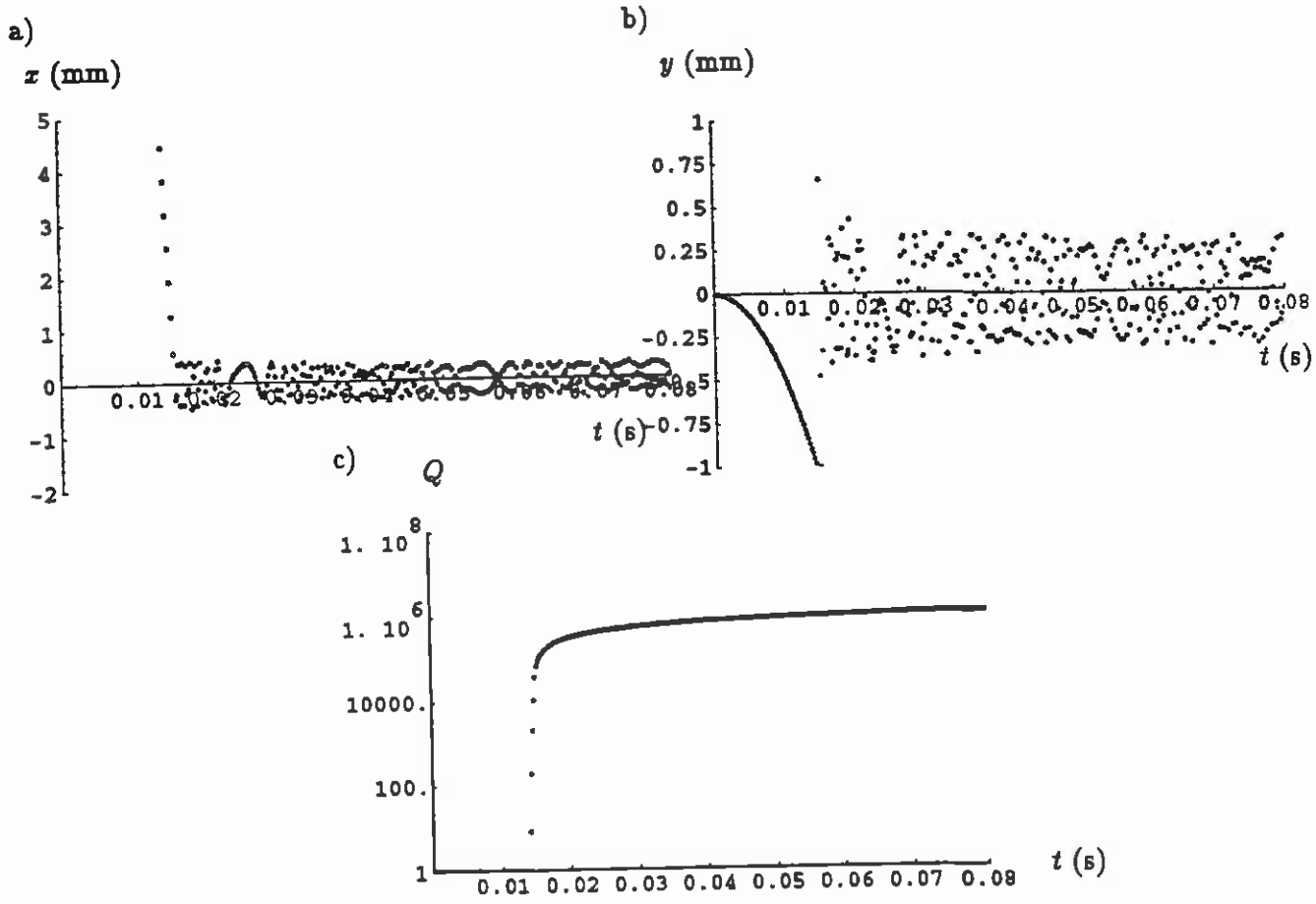

Figure 7: Simulation of capture process in HERA: a) horizontal motion, b) vertical motion, c) charge. Particle is launched at the chamber wall in height of the beam with an initial charge of one and a kinetic energy corresponding to an accelerating (pump) voltage of 5 kV.

7.2 Collection from the Bottom

The average electric force of the electron beam on a particle at the bottom of the vacuum chamber (assuming here $y_{initial} \approx -10$ mm), is about

$$F_{beam} \approx -\frac{N_{cl}^{tot} 2c^2 r_p m_p}{y_{initial} C} \cdot Q \approx \begin{cases} 7.4 \cdot 10^{-18}\, Q \text{ N}, & \text{for HERA} \\ 3.9 \cdot 10^{-16}\, Q \text{ N}, & \text{for the HER} \end{cases} \tag{42}$$

It is proportional to the charge Q of the particle. Notice that for particles already trapped the electric force of the beam is larger by a factor of about $y_{initial}/(\sigma_x + \sigma_y) \sim 10$. This attractive force is opposed by the gravitation

$$F_{grav} \approx -A m_p g \approx 1.7 \cdot 10^{-26}\, A \text{ N} \tag{43}$$

which is proportional to the mass A. In addition, image charge forces have to be considered. For a homogeneously charged spherical particle on a conductive surface the image charge force is

$$F_{image} \approx -\frac{c^2 r_p m_p}{4R^2} \cdot Q^2 1.7 \cdot 10^{-8}\, \frac{Q^2}{A^{\frac{2}{3}}} \text{ N} \tag{44}$$

It increases quadratically as a function of particle charge and is inversely proportional to $A^{\frac{2}{3}}$. The numerical values apply to silicon dioxide. Due to the different dependences on mass and charge of the three forces, it is impossible in HERA and in most other storage rings to pick up any dust particles from the bottom of the beam pipe. This is illustrated in Fig. 8, which shows the absolute value of the three forces on a particle of mass $A = 10^{11}$ in HERA, as a function of the particle charge Q. In order to pick up the particle, the attractive force of the beam has to be larger than the sum of gravity and image charge force. In the case of HERA it is several orders of magnitude lower.

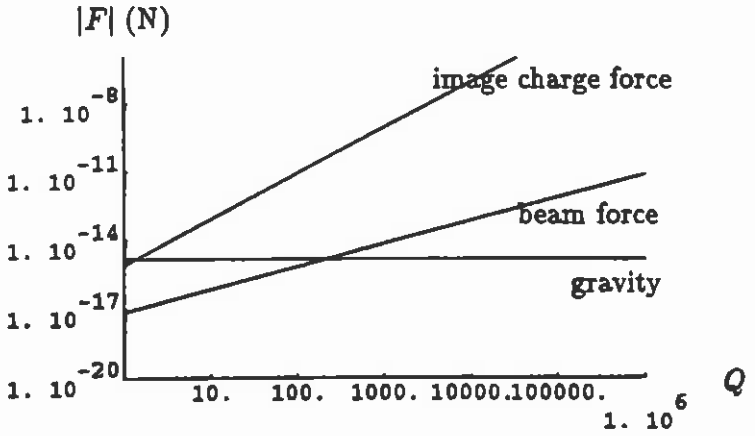

Figure 8: Absolute value of forces acting on a macroparticle of mass $A = 10^{11}$ at the bottom of the beam pipe in HERA, as a function of the particle charge. Gravity and image charge force oppose the attraction by the beam.

Fig. 9 shows the analogous forces for the PEP-II HER at the design beam current of 1 A. The attractive beam force is considerably increased compared with HERA, but an ideal

spherical particle still cannot be trapped. The figure indicates, however, that the margin of safety, which in HERA is at least a factor 100, has shrunk to a factor smaller than 10. It is thus not inconceivable that the electron beam in PEP-II can trap some differently shaped or not homogeneously charged macroparticles from the bottom of the vacuum chamber.

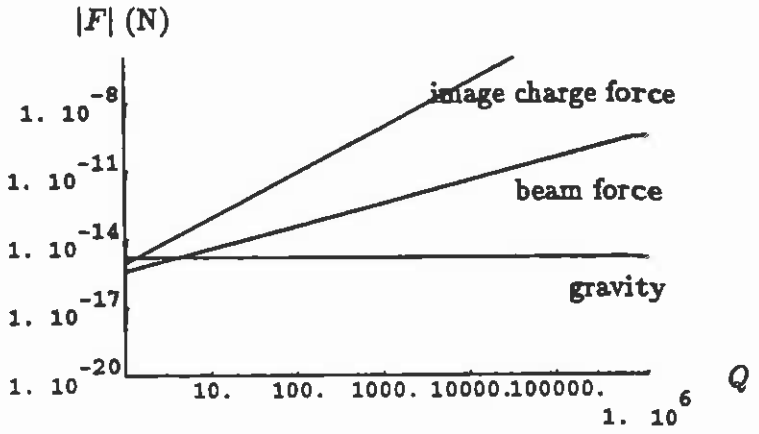

Figure 9: Absolute values of forces acting on a macroparticle of mass $A = 10^{11}$ at the bottom of the beam pipe in the PEP-II HER (current 1A), as a function of the particle charge.

In this section we have only used average forces and ignored the discrete nature of the bunch passages. For the large particles considered this is a sensible approach, as can be seen from a simple estimate: the kick from a single bunch on a macroparticle at the bottom of the beam pipe ($y_{initial} \approx -25$ mm) is

$$\Delta\dot{y} = \frac{N_{el}^{tot} 2 c r_p Q}{n_{bunch} y_{initial} A} \approx \begin{cases} 840 \frac{Q}{A} \frac{\mathrm{m}}{\mathrm{s}}, & \text{for HERA} \\ 910 \frac{Q}{A} \frac{\mathrm{m}}{\mathrm{s}}, & \text{for the HER} \end{cases} \tag{45}$$

which, in the absence of image charge forces and gravity would give rise to a position change during the time interval Δt_d between two bunches of

$$\Delta y = \Delta\dot{y} \cdot \Delta t_d \approx \begin{cases} 80 \frac{Q}{A}\ \mu\mathrm{m}, & \text{for HERA} \\ 3.7 \frac{Q}{A}\ \mu\mathrm{m}, & \text{for the HER} \end{cases} \tag{46}$$

So, as long as $A/Q > 100-1000$, the position change of the particle between two bunches is small compared with its radius, in which case the average forces provide a very good description. Note that for $A = 10^{12}$ the particle charge has to exceed 10^9 before the averaging becomes invalid. For such a high charge, however, the effect of the image charge force is very strong, as reflected in Fig. 8 and 9. For $Q = 10^9$, the image charge forces will dominate even in the unlikely situation that the particle discharges completely after a bunch has passed by. In this context, it should also be mentioned that the maximum photon flux on the chamber wall in PEP-II corresponds to only [31]

$$n_{\gamma,\,wall} \leq 64 \text{ photons / } \mu\mathrm{m}^2 \tag{47}$$

for a single bunch passage. The number of photons hitting the bottom of the pipe will be even smaller. It is thus extremely unlikely, that a particle at the ground of the vacuum chamber can acquire a charge as large as 10^9 without prior discharging.

8 Evaporation Rate and Particle Lifetime

The heating of a macroparticle is completely due to the ionization energy deposited by the electron beam. Compared with which the contribution from synchrotron radiation is negligible as we shall show in the following. If the electrons of the beam are treated as minimum ionizing particles their energy transfer to the macroparticle is written as

$$\left.\frac{\Delta E}{\Delta t}\right|_{ion} = \left(\frac{4}{3}R\right)\frac{R^2}{2\sigma_x\sigma_y}N_{el}^{tot}f_{rev}\cdot\left.\frac{dE}{dx}\right|_{min}\cdot\rho \tag{48}$$

ρ denotes the mass density of the particle and R is its radius (we suppose that the particle has spherical shape); $\frac{4}{3}R$ is the average length traversed by an incident electron inside the dust particle. The energy transfer (48) is proportional to the volume and, thus, increases as the third power of the radius. For a silica particle of density 2.2 g cm^{-3} the deposited energy is

$$\begin{aligned}\left.\frac{\Delta E}{\Delta t}\right|_{ion} &= 2\cdot10^{-5}\frac{A}{10^{13}}\frac{\mathrm{J}}{\mathrm{s}}, \quad \text{for HERA}\\ \left.\frac{\Delta E}{\Delta t}\right|_{ion} &= 3.3\cdot10^{-3}\frac{A}{10^{13}}\frac{\mathrm{J}}{\mathrm{s}}, \quad \text{for the HER.}\end{aligned} \tag{49}$$

The number of photons $N_{\gamma,0}$ hitting the macroparticle per second is roughly

$$N_{\gamma,0} \approx f_{rev}N_{el}^{tot}\sqrt{2\rho_{bend}\sigma_x}\frac{R^2}{2\sigma_x\sigma_y}n_\gamma \approx \begin{cases} 2.7\cdot10^{11}\ \mathrm{s}^{-1}, & \text{for HERA}\\ 1.3\cdot10^{13}\ \mathrm{s}^{-1}, & \text{for the HER}\end{cases} \tag{50}$$

where R, as usual, is the radius of the macroparticle ($R \approx 1\ \mu$m) and n_γ denotes the number of photons emitted per electron per m,

$$n_\gamma \approx \frac{5}{2\sqrt{3}}\frac{\gamma}{137}\frac{1}{\rho_{bend}} \approx 0.8\ \mathrm{m}^{-1}\ \text{, for both HERA and the HER .} \tag{51}$$

The attenuation coefficients in Table 2 along with equation (5) for $x \approx \frac{4}{3}R$ confirm that the dust particle is completely transparent for high-energetic photons. Only photons with low energies, say $E_\gamma \leq 0.1$ keV, are strongly absorbed. To estimate the total energy transfer to the macroparticle by synchrotron radiation, we need the rate of absorbed photons and their typical energy E_γ. For the latter $E_\gamma \approx 0.1$ keV should be a good approximation, while the rate of photons $N_\gamma(E)$ with energies below $E = 0.1$ keV ($E \ll E_{crit}$) is given by

$$\frac{N_\gamma(E)}{N_{\gamma\,0}} \approx \frac{32}{15\sqrt{3}}\left(\frac{E}{E_{crit}}\right)^{\frac{1}{2}} \approx \begin{cases} 0.16, & \text{for HERA}\\ 0.27, & \text{for the HER}\end{cases} \tag{52}$$

The energy transfer due to synchrotron radiation is then approximately

$$\left.\frac{\Delta E}{\Delta t}\right|_{sync} \approx N_\gamma(E)\cdot E_\gamma \approx \begin{cases} 7\cdot10^{-10}\ \mathrm{J/s}, & \text{for HERA}\\ 6\cdot10^{-8}\ \mathrm{J/s}, & \text{for the HER}\end{cases} \tag{53}$$

These numbers are five orders of magnitude smaller than the direct energy deposition by ionization of the electron beam (49). Since the heat capacity of silica is of the order of 73 J/(K mol) from (49) the initial increase in temperature is

$$\frac{\Delta T}{\Delta t} \approx 1\cdot10^{6}\frac{\mathrm{K}}{\mathrm{s}}, \quad \text{for HERA} \tag{54}$$

$$\frac{\Delta T}{\Delta t} \approx 2\cdot10^{8}\frac{\mathrm{K}}{\mathrm{s}}, \quad \text{for the HER ,} \tag{55}$$

independent of R. We have made the assumption that the ionization energy is completely transformed into heat and have ignored fluorescence. The cooling of the dust particle is primarily caused by heat radiation, which is given by an integral over the angular frequency ω of the form

$$\left.\frac{\Delta E}{\Delta t}\right|_{rad} = -\int_0^\infty d\omega \left[\frac{\hbar\omega^3}{\pi c^2(e^{\frac{\hbar\omega}{k_B T}}-1)} R^2\right] \bar{Q}(\omega, R) \tag{56}$$

The expression in square brackets corresponds to the usual Planck spectrum. The absorption coefficient $\bar{Q}_{abs}(\omega, R)$ describes the modification of the Planck formula due to the finite size of the macroparticle. It can be calculated by use of Mie theory [32, 33, 34, 35, 36]. If the absorption coefficient is 1, (56) yields the classical Stefan-Boltzmann result

$$\left.\frac{\Delta E}{\Delta t}\right|_{rad} = -4\pi\epsilon R^2 \sigma_{SB} T^4. \tag{57}$$

Here the symbol ϵ denotes the emissivity, typically $0.3 - 0.8$ (in the following often set equal to one), and $\sigma_{SB} = 5.7 \cdot 10^{-8} \frac{\mathrm{W}}{\mathrm{m^2 K^4}}$ is the Stefan-Boltzmann constant. Note that according to the Stefan-Boltzmann formula the radiated energy is proportional to the surface of the dust particle and, hence, to the square of the radius, which would imply that small particles are always thermally stable.

However, for wavelengths larger than the macroparticle size the heat radiation is suppressed, roughly by a factor $(2\pi R/\lambda)$, λ being the wavelength. In Fig. 10 an approximation to the actual absorption coefficient, as expected from Mie theory [34, 36], is depicted as a function of angular frequency ω for a particle of radius 260 nm. The figure shows the suppression of heat radiation for low frequencies and also that in the transition region to the Stefan-Boltzmann case ($Q \equiv 1$), when the wavelength is about equal to the particle size, the heat radiation is actually enhanced. The approximation of $\bar{Q}(\omega, R)$, used in this report, reads

$$\begin{aligned} \bar{Q}(\omega, R) &= \frac{\omega R}{c}, && \text{for } \omega < \frac{3c}{2R} \\ \bar{Q}(\omega, R) &= 1 + \tfrac{1}{2}\left(\exp\left(-\tfrac{1}{10}\tfrac{\omega R}{c} + \tfrac{3}{20}\right)\right), && \text{for } \omega \geq \frac{3c}{2R} \end{aligned} \tag{58}$$

As a rule of thumb, we can distinguish two regimes as follows

$$\left.\frac{\Delta E}{\Delta t}\right|_{rad} \propto R^3 T^5 \qquad \text{(Mie regime)} \qquad \text{for } TR \ll b \tag{59}$$

$$\left.\frac{\Delta E}{\Delta t}\right|_{rad} \propto R^2 T^4 \qquad \text{(Stefan-Boltzmann regime)} \qquad \text{for } TR \gg b \tag{60}$$

where $b = 2.9 \cdot 10^{-3}$ Km is Wien's constant. It may be anticipated and is more or less evident, that the transition region between these two regimes corresponds to a mass value for which the thermal lifetime $\tau_{part} \equiv A/|\dot{A}|$ of a macroparticle is maximum.

Figure 11 shows a pure Planck radiation spectrum, described by equation (56) with $\bar{Q} \equiv 1$, for a titanium particle of radius 570 nm at temperature 1500 K. Figure 12 illustrates the correct radiation spectrum according to Mie theory (see equation (58)) for the same particle. The low-frequency part of the Planck spectrum is suppressed. From the condition of energy balance

$$\left.\frac{\Delta E}{\Delta t}\right|_{ion} + \left.\frac{\Delta E}{\Delta t}\right|_{rad} \stackrel{!}{=} 0 \tag{61}$$

the equilibrium temperature of a trapped particle is calculated.

In Fig. 13 the equilibrium temperature of a titanium particle trapped in HERA, as obtained from (61), is depicted as a function of particle mass A. All particles of mass up to about $A = 10^{12}$ will acquire the same temperature, which in this particular case roughly equals the melting point of titanium. The evaporation rate and thus the thermal lifetime of a macroparticle is determined by the vapor pressure at this temperature. Figure 14 compares the vapor pressure of different materials. Silica has by far the lowest vapor pressure.

Once the temperature and vapor pressure at this temperature are known, the evaporation rate and thermal lifetime of a macroparticle can be calculated. In thermal equilibrium one knows from kinetic gas theory

$$p = n(v_x^2)_{\rm av} A_{atom} m_p \tag{62}$$

where n denotes the particle density of atoms, 'av' indicates an average over a Boltzmann-distribution and we have

$$m_p A_{atom} (v_x^2)_{\rm av} = k_B T. \tag{63}$$

The thermal emission rate of atoms from the trapped macroparticle is given by

$$j = \frac{1}{2} n |v_x|_{\rm av} \cdot (4\pi R^2) \tag{64}$$

Equations (62) and (63) may be used to eliminate v_x and n in the expression for j, taking into account the relation $|v_x|_{\rm av} = (2(v_x^2)_{\rm av}/\pi)^{\frac{1}{2}}$. The evaporation rate $\dot{A} = (A_{atom} \cdot j)$ is then

$$\dot{A} = -\frac{4\pi A_{atom}}{\sqrt{2\pi m_p A_{atom} k_B}} \left(\frac{3m_p}{4\pi\rho}\right)^{\frac{2}{3}} \frac{p(T)\ [Pa]}{\sqrt{T}} A^{\frac{2}{3}} \approx -8 \cdot 10^5 \frac{p(T)\ [Pa]}{\sqrt{T}} A^{\frac{2}{3}}. \tag{65}$$

Here, the numerical coefficient refers to silica. The thermal lifetime τ_{part} of a macroparticle is given by

$$\tau_{part} \equiv \frac{A}{|\dot{A}|} \tag{66}$$

Fig. 15 illustrates the thermal lifetime obtained from (66) and (65) when using the — incorrect — Stefan-Boltzmann formula (57) for calculating of the equilibrium temperature. For sufficiently small mass, the particles are always expected to be stable. This picture changes substantially, when the correct absorption coefficient $\bar{Q}$ (see Fig. 10) is taken into account. Fig. 16 exhibits a maximum lifetime of a few seconds for masses of the order of 10^{12} proton masses. All other particles will be more unstable and their is no increase of stability, if the particles become smaller by evaporation. The predicted particle lifetime of a few seconds agrees with short drops of the beam lifetime (lasting for typically 10 s), occasionally observed in HERA, but does not provide any explanation for those effects which last for many minutes or hours and are associated with stationary local loss rates.

To understand the latter, our attention may be directed to silica. Fig. 17 shows the temperature of trapped quartz particles in HERA. For masses below $A = 10^{12}$ ($R < 570$ nm) the temperature is again constant. In this case it amounts to about 1490 K, which is well below the melting point ($\sim$ 2000 K). According to Fig. 18, the particles have thermal lifetimes up to 90 hours in this case. Large silica particles trapped by the beam will evaporate rapidly until they reach a mass of the order of $A = 10^{12} - 10^{13}$, where they will stabilize. This process provides a simple explanation why the measured beam lifetime always drops to about the same value and

does not show large variations. The equilibrium temperature of trapped particles (with masses below $\sim 10^{12}$) would become equal to the melting point roughly at the design current of 55 mA. It is thus possible, if not likely, that for the design current the beam lifetime problem in HERA will disappear.

Fig. 19 shows the extrapolation to the PEP-II HER for the most stable material, silica. The equilibrium temperature expected from Mie theory is 4150 K, if the mass is smaller than 10^{11}. Performing the same calculation as for HERA, we find the thermal lifetimes shown in Fig. 20, which for the mass range of interest are smaller than 10 μs. It is questionable, however, if the same formulae as for HERA really do apply: since the temperature is much larger than the melting point, the particle will explode after a short time, during which it is heated and charged. We will see shortly that coincidentally for PEP-II this latter time is also of the order 10 μs.

After having derived an expression for the heat evaporation rate (65), we are in a position to make a consistency check of the field evaporation rate (32). The ratio of evaporated ions and neutral atoms is given by the Saha-Langmuir equation [38, 39, 40, 41, 42], which implies for our case

$$\frac{\dot{Q} A_{atom}}{\dot{A}} \stackrel{!}{=} A_+ \exp\left(-\frac{U+V-\Phi_-}{k_B T} + \frac{e^2\sqrt{Q}}{4\pi\epsilon_0 R k_B T}\right) \tag{67}$$

where A_+ is a constant or order one. Fig. 21 compares the expressions on the left and right hand side of (67) for $A_+ = 1$. The Saha-Langmuir prediction is larger by a factor of order 10-100. This difference is not significant for the determination of the equilibrium charge. It is mainly due the factor A_+, which is not exactly one, but, for titanium,

$$A_{+,\,Ti} = \frac{g_{ion}}{g_{atom}} = \frac{2}{9} \approx 0.2. \tag{68}$$

Here g_{atom} and g_{ion} denote the statistical weight of atoms and ions, respectively. A small error has also been made in approximating the double integral over the heat capacity in (33).

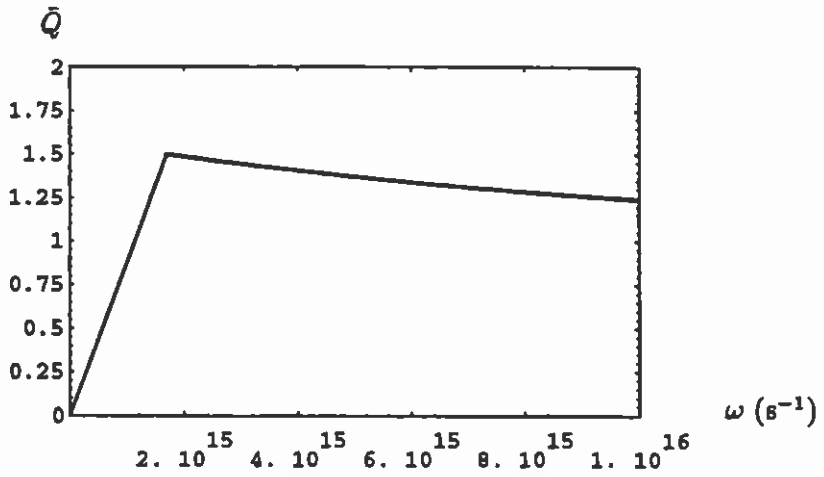

Figure 10: Absorption coefficient $\bar{Q}(\omega, R)$ used in the calculation versus the angular frequency ω in s^{-1} for a spherical particle of radius $R = 264$ nm ($A = 10^{11}$ for titanium). The function $\bar{Q}(\omega, R)$ represents an approximation to Mie theory [34].

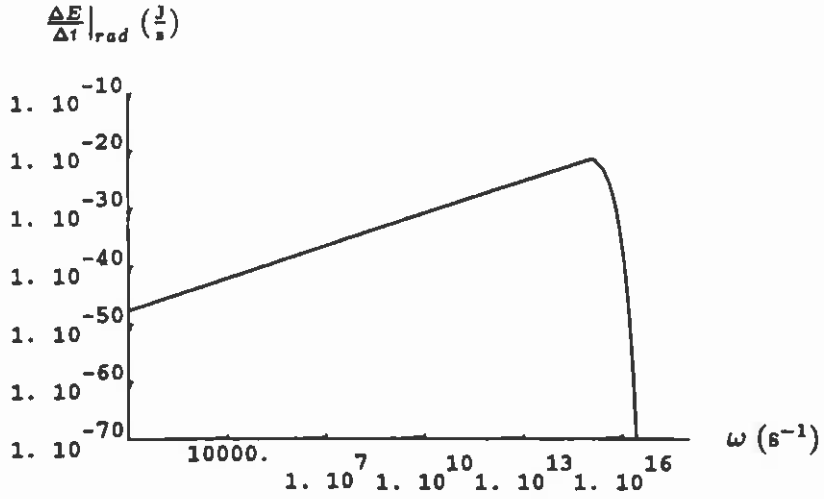

Figure 11: Heat radiation spectrum $\Delta E/\Delta t$ (ω) according to Planck for a titanium particle of radius $R = 570$ nm ($A = 10^{12}$) and temperature 1500 K.

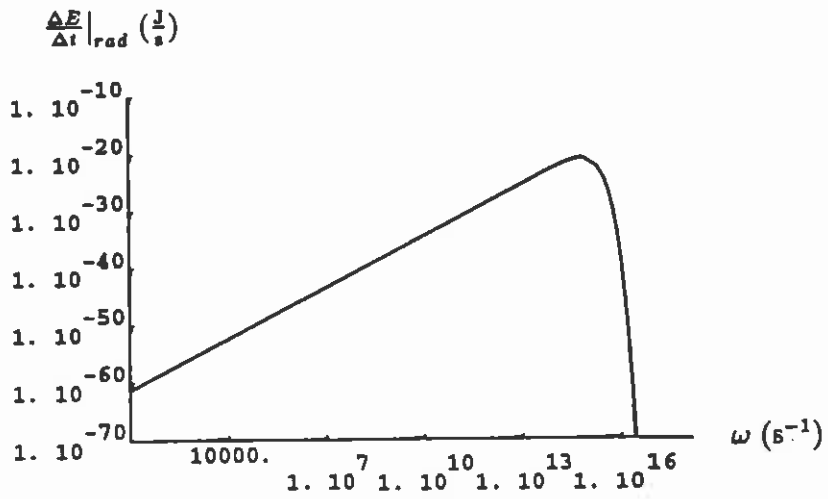

Figure 12: Heat radiation spectrum $\Delta E/\Delta t\ (\omega)$ according to Mie theory for a titanium particle of radius $R = 570$ nm ($A = 10^{12}$) and temperature 1500 K.

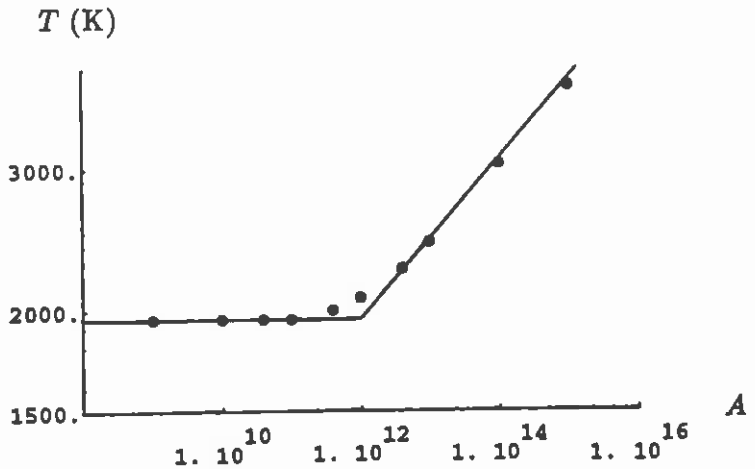

Figure 13: Temperature of titanium macroparticle as a function of particle mass A for HERA.

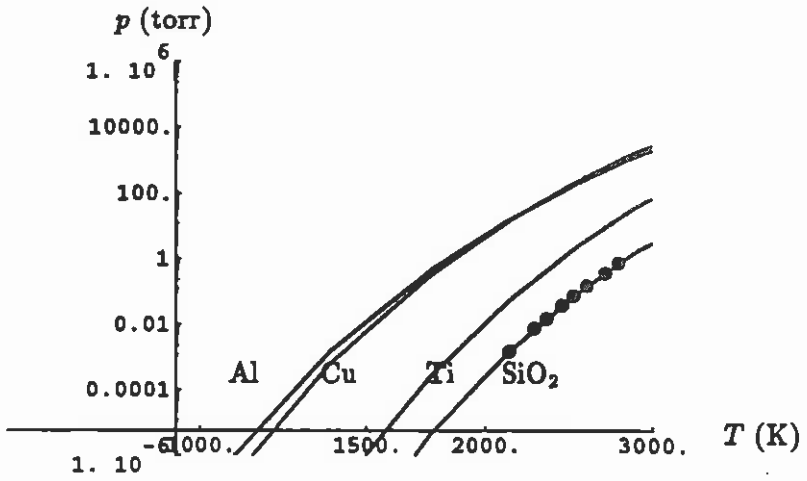

Figure 14: Vapor pressure as a function of temperature for aluminum, copper, titanium and silica. Silica is the most stable of these materials.

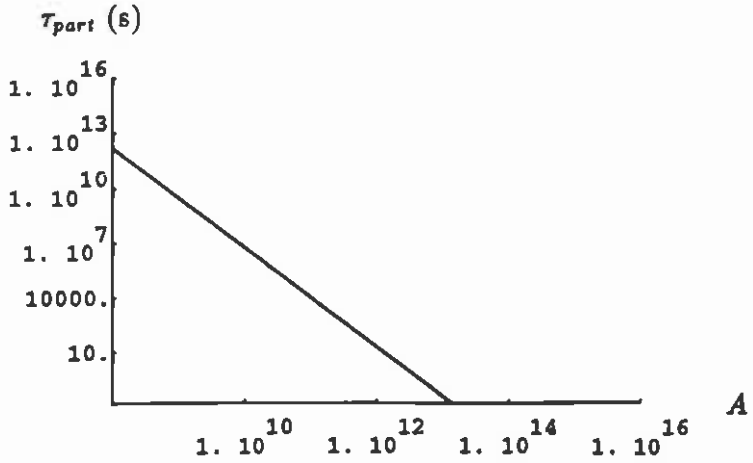

Figure 15: Incorrect thermal lifetime $\tau_{part} \equiv A/|\dot{A}|$ of titanium macroparticle in HERA as a function of particle mass A according to Planck/Stefan-Boltzmann theory.

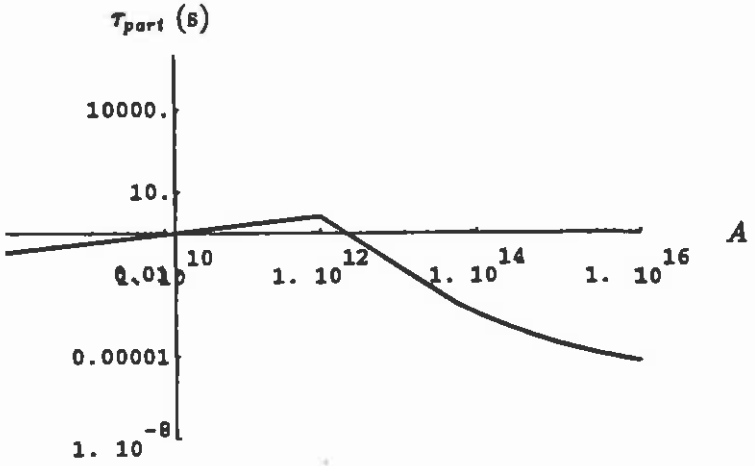

Figure 16: Thermal lifetime $\tau_{part} \equiv A/|\dot{A}|$ of titanium macroparticle in HERA as a function of particle mass A according to Mie theory.

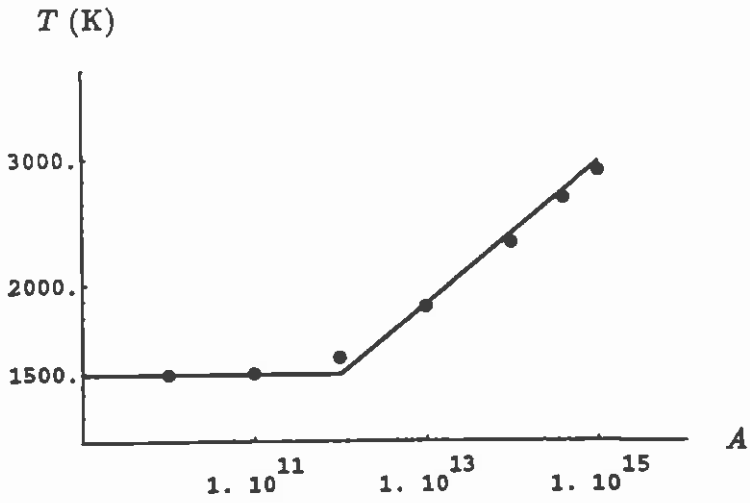

Figure 17: Temperature of silica macroparticle as a function of particle mass A for HERA.

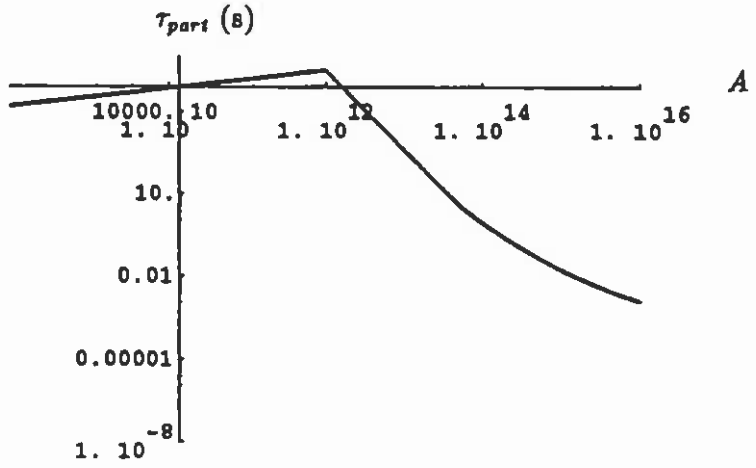

Figure 18: Thermal lifetime $\tau_{part} \equiv A/|\dot{A}|$ of silica macroparticle in HERA as a function of particle mass A according to Mie theory.

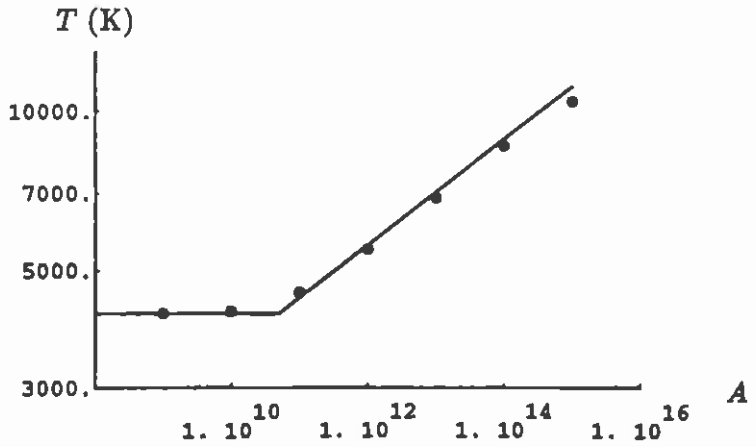

Figure 19: Temperature of silica macroparticle as a function of particle mass A for the PEP-II High Energy Ring.

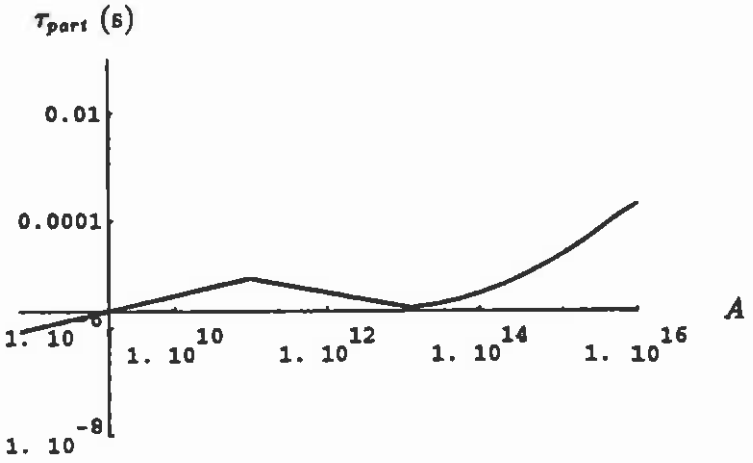

Figure 20: Thermal lifetime $\tau_{part} \equiv A/|\dot{A}|$ of silica macroparticle in the PEP-II HER as a function of particle mass A according to Mie theory.

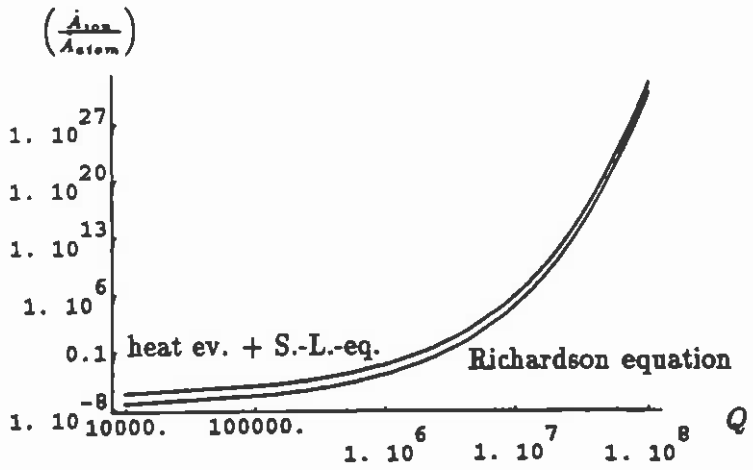

Figure 21: Comparison of field evaporation discharging rate calculated directly from the Richardson equation (32) with that obtained from heat evaporation rate $\dot{A}/A$ (65) plus Saha-Langmuir equation (67).

9 Cooling by Evaporation and Destruction Rates

We have tacitly assumed, that the cooling by heat radiation is much larger than the cooling by evaporation. The latter becomes important, however, when the evaporation rate approaches a value of the order

$$\left(\frac{\dot{A}}{A}\right) = \left(\frac{\Delta E}{\Delta t}\right)_{ion} \frac{1}{V \cdot A} A_{atom} \tag{69}$$

where V denotes, as before, the evaporation energy per atom (4.9 eV for titanium). For a titanium particle, one estimates from this cooling mechanism

$$\tau_{part} > 4 \text{ ms} \quad \text{or } \frac{\dot{A}}{A} < 226 \text{ s}^{-1} \quad \text{in HERA} \tag{70}$$

$$\tau_{part} > 48 \ \mu\text{s} \quad \text{or } \frac{\dot{A}}{A} < 21\,000 \text{ s}^{-1} \quad \text{in the PEP-II HER} \tag{71}$$

These numbers give the minimum possible thermal lifetimes of trapped macroparticles consisting of titanium, if they are not melting. Similar values may be expected for quartz particles. An interesting question is the fate of a dust particle after it is trapped in PEP-II. After 9 μs its temperature reaches the melting point of about 2000 K, from (55). According to (27) and (35), at that moment it has acquired a charge $Q \approx 3 \cdot 10^5$ so that it explodes. A minimum velocity of the remnant atoms may be estimated from a Boltzmann-distribution,

$$v_{atom,\ \mathrm{rms}} \approx \left(\frac{kT}{m_p A_{atom}}\right)^{\frac{1}{2}} \approx 600 \ \frac{\mathrm{m}}{\mathrm{s}} \tag{72}$$

and the atoms will then have left the beam region after roughly

$$\Delta t \approx \frac{\sqrt{\sigma_x \sigma_y}}{v_{atom,\ \mathrm{rms}}} \approx 630 \text{ ns}. \tag{73}$$

This time has to be compared with the typical time required for ionization, which is

$$\tau_{ioniz} \approx \frac{2\pi \sigma_x \sigma_y C}{N_{el}^{tot} c \sigma_{coll}} \approx 660 \ \mu\text{s} \tag{74}$$

where $\sigma_{coll} \approx 2 \cdot 10^{-22}$ m^2 is the cross section for collisional ionization [43]. Hence, it is safe to assume that the atoms will disappear immediately and ignore their effect on the beam lifetime. For completeness, it should be mentioned that single-atomic ions would stay in the beam typically for about 2–4 revolution times (10–20 μs). We have thus found that the capture of a single dust particle in the beam reduces the beam lifetime for a period of about 10 μs, after which the macroparticle explodes. Its remnants are lost immediately. Based on this value one can estimate the maximum tolerable number of dust particles in PEP-II, or the rate at which those particles can be destroyed.

Assuming that the beam average current is 1 A and that every 10 μs a dust particle is annihilated and a new one captured, the maximum destruction rate for continually produced particles is estimated as

$$\dot{N}_{part,\ \mathrm{av}} = 6 \cdot 10^{10} \ \frac{1}{\text{week}} \tag{75}$$

corresponding to a maximum density of particles at the bottom of the beam pipe of

$$\dot{\rho}_{surf,\ \mathrm{av}} = 300 \ \frac{1}{\text{mm}^2 \cdot \text{week}}. \tag{76}$$

These numbers apply independently of the mass of the trapped macroparticles. For masses $A \approx 10^{12}$ the effect on the beam lifetime would be not measurable compared with the residual gas lifetime, for $A \approx 10^{14}$ the beam lifetime would be about 30 min.

As a worst case, one might consider the possibility that at the first injection of beam all dust particles lying on the bottom of the chamber are simultaneously trapped by the beam. If one requires for this case that the beam lifetime is at least equal to the particle lifetime, one finds a maximum destruction rate of

$$N_{part,\ initial} \approx 2 \cdot 10^8 \tag{77}$$

or

$$\rho_{surf,\ inital} \approx 1\ \frac{1}{\mathrm{mm}^2} \tag{78}$$

for a current of 1 A and dust particles of radius 500 nm ($A = 10^{12}$). A more stringent requirement is that the beam lifetime should be at least equal to the injection time. In PEP-II, it is possible to inject a current of 1 A within roughly 20 s. Choosing this value for the beam lifetime, we find the much smaller number

$$N_{part,\ initial} \approx 100 \tag{79}$$

or

$$\rho_{surf,\ initial} \approx 5 \cdot 10^{-7}\ \frac{1}{\mathrm{mm}^2}. \tag{80}$$

It appears, however, very unlikely that all dust particles are trapped within a few microseconds after injection. Experience at HERA suggests that it takes several minutes and sometimes even an hour before only one macroparticle is trapped. One precaution aimed for at PEP-II is a clean assembly of the vacuum chamber and its components, to minimize the number of dust particles in the beam pipe.

10 Copper-Sputtering Scenario

Before results are summarized and some conclusions are drawn, a short digression from macroparticles to single atoms may be worthwhile. When the drop of the beam lifetime was first observed in the summer of 92, the much higher sputtering yield of copper compared with aluminum indicated a possible explanation of the bad beam lifetime [44]. The same idea has been revitalized more recently when it was suggested [45] that in PEP-II copper-sputtering on the vacuum chamber wall could give rise to an avalanche-like generation of atoms and ions, even if that is not the cause of the problem in HERA. The scenario would be roughly as follows. Some atoms of the residual gas are ionized by the beam. Since they are unstable they get lost and hit the vacuum chamber wall, where they release new atoms by sputtering. These new atoms could again be ionized by the beam or by synchrotron radiation, become unstable and get lost at the wall. For certain parameter values an avalanche-like process would be conceivable. Obviously the necessary condition for avalanche is

$$\text{(sputtering yield per ion)}\ \mathrm{X}\ \text{(probability of ionization)}\ \geq 1 \tag{81}$$

The sputtering yield strongly depends on the energy of the incident ions. It increases with energy and reaches some saturation value for ion energies larger than 10 keV [46, 47, 48]. The

self-sputtering yield for copper at 45 keV is about 8, while the self-sputtering yield for aluminum is only ~ 0.5. To estimate the energy of lost ions a simulation study has been performed, in which a few hundred unstable particles were launched at different initial vertical positions and tracked until they were lost on the chamber wall. The loss usually happens within a few revolution times. The kinetic energy at the moment of loss is calculated and recorded. A typical result for fully ionized copper ions ($A/Q = 2$) in the Low Energy Ring (LER) is shown in Fig. 22. As far as this simulation is concerned, the LER differs from the HER only by its two times higher beam current (2 A), and can, therefore, be considered as a worst case. In the example of Fig. 22 the horizontal initial amplitude was chosen as about zero. As one can see, the ion energies show a considerable spread, independently of the vertical starting amplitude, but do not exceed values of about 300 eV.

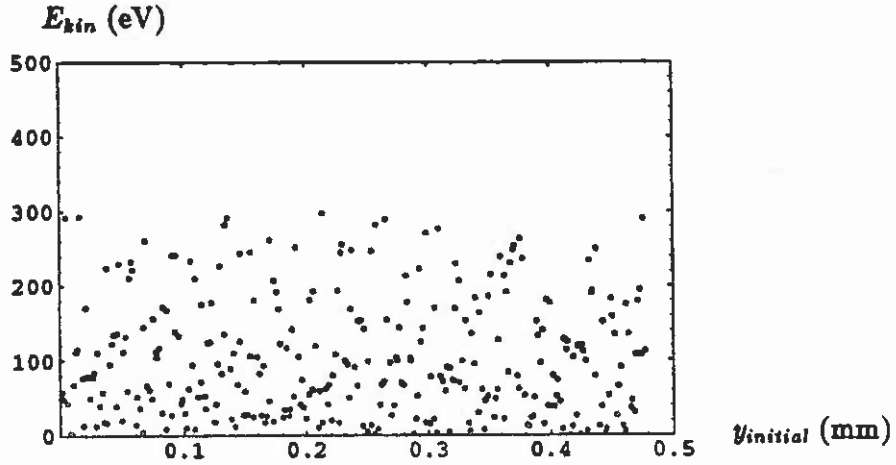

Figure 22: Kinetic energy of copper ions hitting the vacuum chamber wall for mass-to-charge ratio $A/Q = 2$ and various initial vertical starting amplitudes ($x_{initial} \approx 0$), as predicted by a simulation for the PEP-II LER.

In Table 3 average and rms-value of the ion energy is compared for two different states of ionization (fully ionized and single-charged copper atoms) and for two different initial horizontal positions. The simulation has been performed with the nonlinear kick of a round beam. Two different values have been used for the round-beam sigma σ_r. The Table shows that the energy of lost ions is always of the order 100 ± 100 eV and is highly insensitive to any of these parameters. Indeed, almost the same values have been found for the HER and for HERA. From the literature [46, 47, 48] the sputtering yield for 100 eV ions on copper varies between 0.2 and about 1.

It is well known [46, 47], that about 99 % of the sputtered atoms are neutral. Hence to cause an avalanche effect, they have to be ionized by the beam or the radiation. The velocity distribution of atoms sputtered from a copper surface for an incident ion energy of 100 eV shows a maximum at $v_{atom} \approx 3 \cdot 10^3$ m/s (corresponding to a kinetic energy of about 6 eV). During one revolution period such atoms would travel a transverse distance of about 35 mm, comparable to the chamber radius. The cross section for collisional ionization is about [43, 49] $\sigma_{coll.} \approx 2 \cdot 10^{-22}$ m^2 and the probability for ionziation by the beam becomes

$$p_{beam} < \frac{N_{el}^{tot}}{2\pi\sigma_x\sigma_y} \cdot \frac{2\sigma_x}{v_{atom} t_{rev}} \cdot \sigma_{coll.} \approx 0.002 \tag{82}$$

A/Q	σ_r	x_{start}	kinetic energy [eV]	σ_E [eV]
64	σ_y	0	120	117
64	σ_y	σ_x	98	96
2	σ_y	0	102	79
2	σ_y	σ_x	119	90
2	σ_x	0	91	76
2	σ_x	σ_x	121	110

Table 3: Kinetic energy of lost ions in the PEP-II LER for different ionization states and horizontal starting amplitudes, and for two values of the round-beam size used in the simulation. Each row gives the average and rms-spread over a few hundred ions, for which the initial vertical amplitude is distributed between 0 and $3\sigma_y$ ($\sigma_y \approx 0.16$ mm in the LER).

The first factor is the projected density of electrons or positrons at the bunch center for one revolution period, while the second represents the fraction of time required to traverse a distance of $2\sigma_x$.

The atoms can also be ionized by synchrotron radiation. For a current of 1 A the photon generation rate in the HER is supposed to be [31] $\tilde{N}_{\gamma,0} \approx 7.1 \cdot 10^{18}$ photons/(s·m) and the flux of photons hitting an atom would be

$$j_\gamma \approx \tilde{N}_{\gamma,0} \frac{\sqrt{2\rho_{bend}\sigma_x}}{2\pi\sigma_x\sigma_y} \approx 4.2 \cdot 10^{24} \frac{1}{\mathrm{sm}^2} \tag{83}$$

where $\rho_{bend} \approx 165$ m is the bending radius of a dipole magnet.

A value $\sigma_{rad} \approx 2 \cdot 10^{-22}$ m^2 should also be a reasonable upper bound for the cross section of photo-electric ionization, integrated over the photon spectrum of the synchrotron radiation (compare, for instance, Ref. [50]; this value corresponds to $3 \cdot 10^6$ times the Thomson cross section $8\pi r_e^2/3$, which is the total cross section for scattering on a free charge). We then arrive at

$$p_{rad} \approx j_\gamma \sigma_{rad} t_{rev} \approx 0.006 \tag{84}$$

for the PEP-II HER. The total probability of ionization is thus not larger than 1%.

Since the sputtering yield for typical energies of lost ions is barely one, and the ionization probability of sputtered atoms smaller than 1%, we find that an avalanche effect of copper-sputtering is impossible in PEP-II.

11 Summary and Conclusions

A consistent theory has been developed which explains the beam lifetime problem encountered at HERA by the capture of single macroparticles, made from silicon dioxide. Typically the mass of a trapped particle is $A \approx 10^{12} - 10^{13}$ ($R \approx 500$ nm–1 μm) and its equilibrium charge about 10^7. It was shown that such particles are dynamically and thermally stable, and that all observations are consistent with this model. The reduction of beam lifetime is most likely caused by bremsstrahlung in the external field of the charged particle ('duststrahlung'). The origin of the macroparticles is not completely understood, but related to the distributed ion pumps in the dipole magnets.

Extrapolation to PEP-II shows that the lifetime of trapped macroparticles in the HER will be only 10 μs. Hence, the effect on the beam lifetime is insignificant provided that the production rate of such particles is not many orders of magnitude higher than in HERA and that the beam pipe is not too polluted. In PEP-II special emphasis will be given to a clean assembly of the vacuum chamber, and the pumps will very likely be built in a reversed-ground design. Given these precautions, dust trapping should be no problem for PEP-II.

Acknowledgements

I am very grateful to J. Seeman, W. Stoeffl and M. Zolotorev for several stimulating discussions and many valuable suggestions. I am also indebted to R. Brinkmann for providing some recent informations from HERA.

References

[1] F. Zimmermann, "Trapped Dust in HERA and DORIS", *DESY HERA* **93-08** (1993).

[2] S. Schlögl and K. Wittenburg, "A Beam Loss Monitor System for HERA", *Proceedings of the 1992 High Energy Accelerator Conference, Hamburg* 254 (1992).

[3] K. Wittenburg, "Preservation of Beam Loss Induced Quenches, Beam Lifetime and Beam Loss Measurements with the HERA-p Beam-Loss-Monitor-System", *DESY* **94-003** (1994).

[4] R. Brinkmann, private communications (1994).

[5] H. Saeki, T. Momose and H. Ishimaru, "Observations of Dust Trapping Phenomena in the TRISTAN Accumulation Ring and a Study of Dust Removal in a Beam Chamber", *Rev. Scient. Instr.* **62** No.4 874 (1991).

[6] H. Saeki, T. Momose and H. Ishimaru, "Motions of Trapped Dust Particles Around the Electron Beam in the TRISTAN Accumulation Ring", *Rev. Scient. Instr.* **62** No.11 2558 (1991).

[7] P. Marin, "Observation of Bremsstrahlung on Dust Particles Trapped in Electron Beams at DCI and Super-ACO", *LURE-RT/91-03* (1991).

[8] D. Sagan, "Mass and Charge Measurement of Trapped Dust in the CESR Storage Ring", *NIM* **A330** 371 (1993).

[9] E. Jones, F. Pedersen, A. Poncet, S. van der Meer, E. J. N. Wilson, "Transverse Instabilities Due to Beam-Trapped Ions and Charged Matter in the CERN Antiproton Accumulator", *CERN/PS/85-15 (AA)* (1985).

[10] M. Placidi, private communication (1994).

[11] Particle Data Group, "Review of Particle Properties", *Phys. Review D* **45** (1992).

[12] "CRC Handbook of Chemistry and Physics", 68th edition, CRC Press, Inc., Boca Raton, p. D-185 (1987).

[13] E.U. Condon and H. Odishaw, "Handbook of Physics", 2nd edition, McGraw-Hill (1967).

[14] G.W. Kaye and T.H. Laby, "Tables of Physical and Chemical Constants", Longman (1973).

[15] Landolt-Boernstein, "Zahlenwerte und Funktionen aus Naturwissenschaften und Technik", Vol. **2**, Springer-Verlag, Heidelberg (1961).

[16] H.L. Anderson (ed.), "A Physicist's Desk Reference", AIP, New York (1981).

[17] A. Piwinski, "Beam losses and lifetime", CERN Accelerator School, Gif-sur-Yvette 1985, *CERN* **85-19** (1985).

[18] The name was suggested by J. Seeman (1994).

[19] A.A. Sokolov and I.M. Ternov, "Radiation from Relativistic Electrons", AIP, Translation Series, New York (1986).

[20] K. Yokoya and P. Chen, "Beam-Beam Phenomena in Linear Colliders", *KEK* **91-002** (1991).

[21] Y. Baconnier and G. Brianti, "The Stability of Ions in Bunched Beam Machines", *CERN/SPS/80-2* (DI) (1980).

[22] M. Bassetti and G. A. Erskine, "Closed Expression for the Electrical Field of a Two-dimensional Gaussian Charge", *CERN-ISR-TH/80-06* (1980).

[23] M. Zolotorev, private communication (1994).

[24] F. Pedersen, "Effects of Highly Charged, Solid Microparticles Captured in Negatively Charged Circulating Beams", *CERN PS/87-25* (1987).

[25] M. Zolotorev, private communication (1994).

[26] D.K. Davies and M.A. Biondi, "The effect of electrode temperature on vacuum electrical breakdown between plane-parallel copper electrodes", J. Appl. Phys. **39** no 7 p. 2979 (1968).

[27] T. Utsumi and J.H. English, "Study of electrode products emitted by vacuum arcs in form of molten metal particles",*J. Appl. Phys.* **46** no 1, p. 127 (1975).

[28] J.E. Daalder, "Components of cathode erosion in vacuum arcs", *J. Phys. D* Vol. **9** p. 2379 (1976).

[29] G.A. Mesyats and D.I. Proskurovsky, "Pulsed electric discharge in vacuum", Springer-Verlag (1989).

[30] W. Stoeffl and J. Seeman, private communication (1994).

[31] "PEP-II, An Asymmetric B-Factory", Conceptual Design Report, *SLAC-418* (1993).

[32] K. Flöttmann, private communication (1993).

[33] W. Stoeffl, private communication (1994).

[34] D.J. Lien, "Dust in Comets. I. Thermal Poperties of Homogeneous and Heterogeneous Grains", Astroph. J. **355** p. 680 (1990).

[35] R. Scholl and B. Weber, "Die Cluster-Lampe: Eine neue Art, Licht zu erzeugen", Phys. Bl. **48** p. 729 (1992).

[36] C.F. Bohren and D.R. Huffmann, "Absorption and Scattering of Light by Small Particles", Wiley, New York (1983).

[37] J.W. Mellor, "A Comprehensive Treatise on Inorganic and Theoretical Chemistry", J. Wiley, New York (1922).

[38] K. Compton and I. Langmuir, "Electrical Discharges in Gases, Part I. Survey of Fundamental Processes", *Rev. Mod. Phys.* **2**, 123 (1930).

[39] I. Langmuir, "Caesium Films on Tungsten", *J. Am. Phys. Soc.* **44**, 1252 (1932).

[40] P.A. Redhead, J.P. Hobson, E.V. Kornelsen, "The Physical Basis of Ultrahigh Vacuum", AIP, New York (1993).

[41] M. Harwit, "Astrophysical Concepts", Springer-Verlag (1988).

[42] M. Zolotorev, private communication (1994).

[43] T.O. Raubenheimer and P. Chen, "Ions in the Linacs of Future Linear Colliders", *SLAC-PUB*-**5893** (1992).

[44] D. Degèle and D. Trines, private communication (1992).

[45] W. Stoeffl, private communication (1993).

[46] R. Behrisch (ed.), "Sputtering by Particle Bombardment", I–III, Springer-Verlag, Berlin (1983).

[47] M. Kaminsky, "Atomic and Ionic Impact Phenomena on Metal Surfaces", Springer-Verlag, Berlin (1965).

[48] G. Carter and J.S. Colligon, "Ion Bombardment of Solids", American Elsevier Publ. Comp., Inc., New York (1968).

[49] F.F. Rieke and W. Prepejchal, "Ionization cross sections of gaseous atoms and molecules for high energy elelctrons and positrons", *Phys. Rev. A* **6** (1972).

[50] W. Heitler, "The Quantum Theory of Radiation", Clarendon Press (1954).